ISCI, Volume *23*

Supplemental Information

Controlling Deoxygenation Pathways in Catalytic Fast Pyrolysis of Biomass and Its Components by Using Metal-Oxide Nanocomposites

Anqing Zheng, Zhen Huang, Guoqiang Wei, Kun Zhao, Liqun Jiang, Zengli Zhao, Yuanyu Tian, and Haibin Li

Supplemental Figures

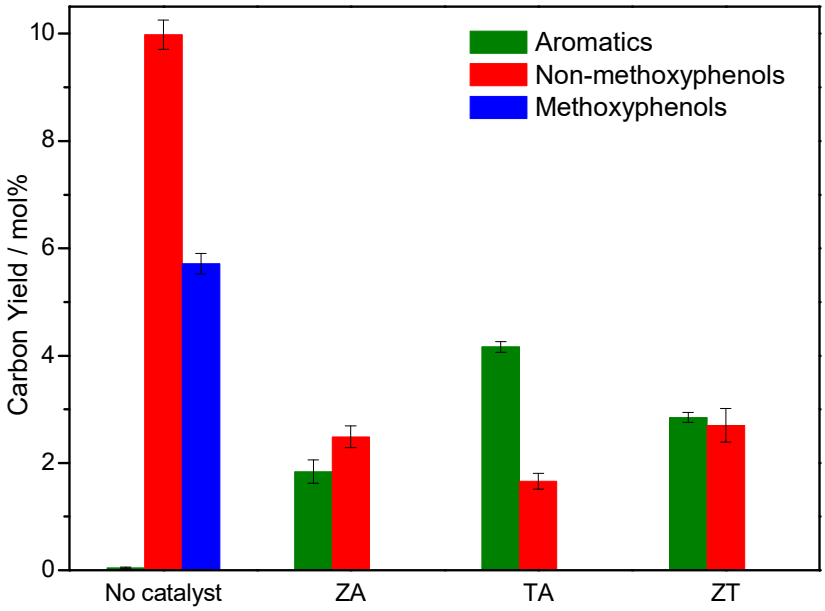

Figure S1 The carbon yields of aromatics and phenols from catalytic fast pyrolysis of organosolv lignin derived from bagasse over different nanocomposites, related to Figure 4.

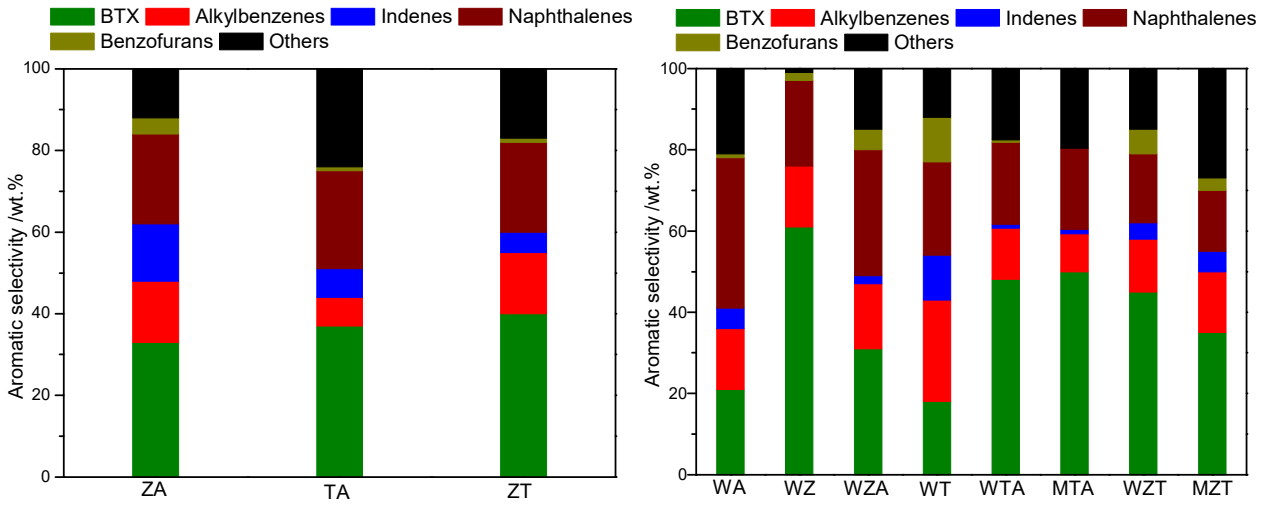

Figure S2 The aromatic selectivity from catalytic fast pyrolysis of organosolv lignin derived from bagasse over different nanocomposites, related to Figure 4.

BTX: benzene, toluene and xylenes; Alkylbenzenes: ethylbenzene, ethyltoluenes, ethylxylenes, trimethylbenzenes, tetramethylbenzenes, pentamethylbenzene; Indenes: Indene, methylindenes; Naphthalenes: naphthalene, methylnaphthalenes, ethylnaphthalenes, dimethylnaphthalenes, trimethylnaphthalenes; Benzofurans: benzofuran, methylbenzofurans; Others: fluorene, methylfluorenes, anthracene, methylanthracenes, phenanthrene, methylphenanthrenes.

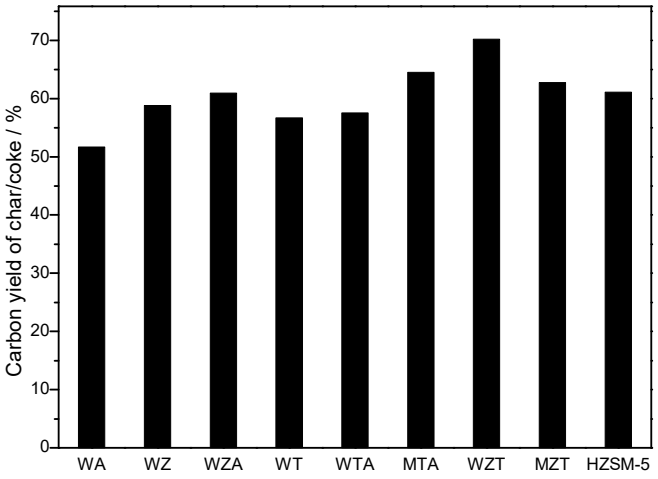

Figure S3 The yields of char/coke from the CFP of organosolv lignin derived from bagasse over different nanocomposites, related to Figure 4.

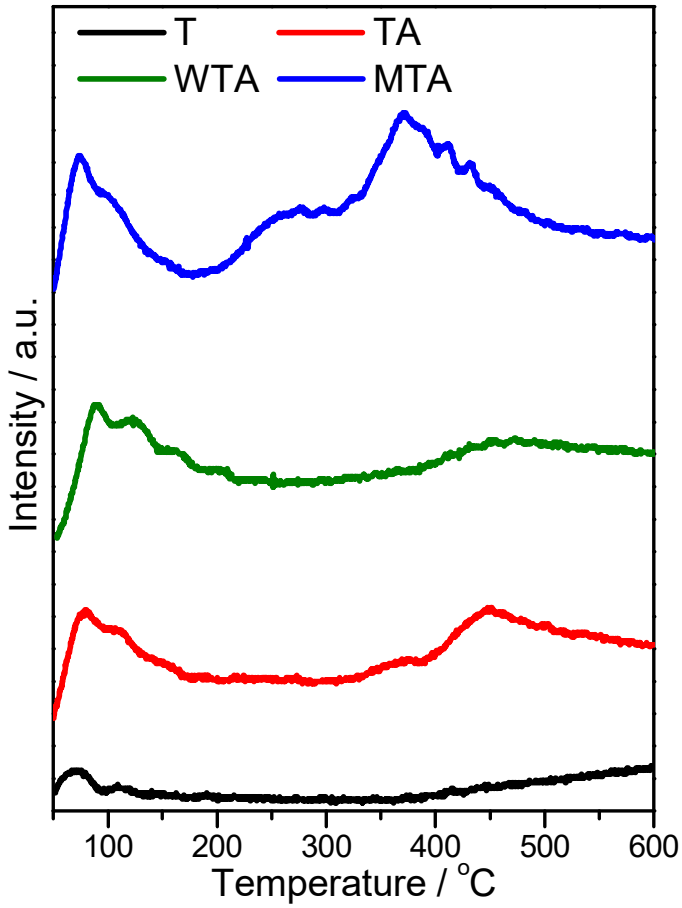

Figure S4 CO_2-TPD profiles of different nanocomposites, related to Figure 7.

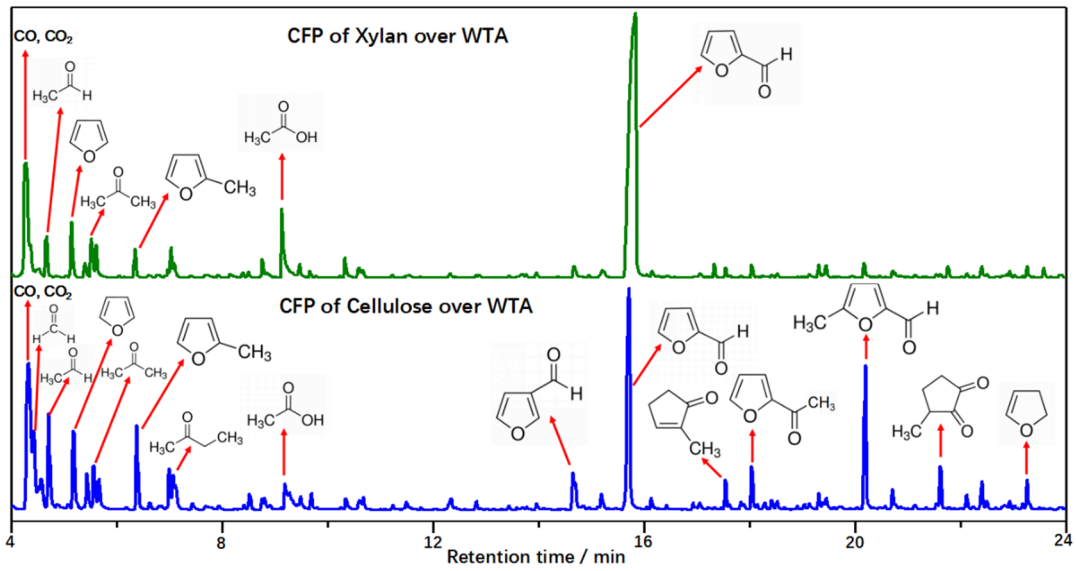

Figure S5 Total ion chromatograms resulting from the CFP of xylan and cellulose over WTA at 600 °C with a catalyst-to-feedstock weight ratio of 3, related to Figure 8.

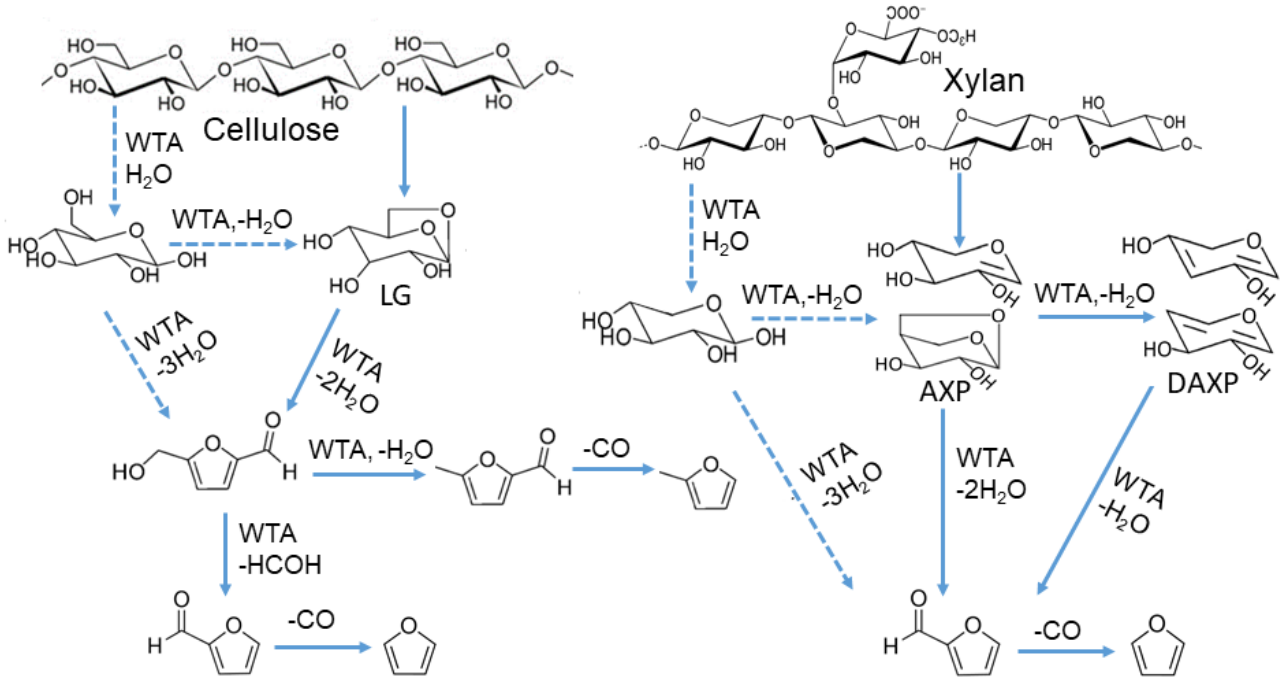

Figure S6 Possible reaction pathways for the formation of furans from the CFP of xylan and cellulose over WTA, related to Figure 8.

Supplemental Tables

Table S1 The yields of aromatics from the CFP of biomass and its components in literature, related to Figure 4 and Figure 10.

Feedstocks	Catalyst	Carbon yield of aromatics	Reference
Lignin	HZSM-5	2-9%	(Wang et al., 2014)
Lignin	CoO/MoO_3 and HZSM-5	Up to 6.2%	(Mullen and Boateng, 2010)
Lignin, cellulose and biomass	HZSM-5 and H-Beta	1-14%	(Mihalcik et al., 2011)
Red oak	HZSM-5	14.5-17.7%	(Wang et al., 2015)
Lignin	HZSM-5	13.38-27.91% (relative peak area)	(Lee et al., 2016)
Pine	MoO_3/TiO_2	7%	(Murugappan et al., 2016)
Pine	$Ti(SO_4)_2$-Mo_2N/HZSM-5, Mo_2N/HZSM-5	Up to 13.63 wt.%	(Lu et al., 2019)
Pine	ZnAl, Zn_2Al, MgAl, Mg_2Al	Up to 4% (relative peak area)	(Edmunds et al., 2019)
Lignin and biomass	WO_3-TiO_2-Al_2O_3	Up to 8.5% for lignin and 14.7% for pine	This work

Table S2 The yields of furans from the CFP of biomass and its components in literature, related to Figure 8 and Figure 10.

Feedstocks	Catalyst	Yield of furfural or furans	Reference
Corncobs	$Fe_2(SO_4)_3$, H_2SO_4, $ZnCl_2$	5–6 wt.%%	(Branca et al., 2012)
Corncobs	H_2SO_4	0.65-5% wt.%	(Branca et al., 2011)
Biomass, cellulose, and xylan	$ZnCl_2$	Up to 70% (relative peak area)	(Lu et al., 2011)
Bagasse	$CuSO_4$/HZSM-5	28% (relative peak area)	(Zhang et al., 2014)
Cellulose	ZrCu-SAPO-18 ZrCu-SAPO-34	Selectivity of 63.86% (relative peak area)	(Chen et al., 2018)
Xylan, cellulose and biomass	WO_3-TiO_2-Al_2O_3	Up to 29.9% for xylan, 17.7% for cellulose and 20.5% for eucalyptuses (carbon yield)	This work

Transparent Methods

Preparation and characterization

The metal-oxide nanocomposites were synthesized by a coprecipitation method. A stable aqueous $TiCl_4$ solution was prepared by dissolving the desired amount of $TiCl_4$ in deionized water with vigorous stirring in an ice-water bath. The W- or Mo-free nanocomposites were precipitated from a mixture of Al $(NO_3)_3 \cdot 9H_2O$, $TiCl_4$ or $ZrOCl_2 \cdot 8H_2O$ with different metal-to-metal molar ratios (1:1 for a binary mixture and 1:1:1 for a ternary mixture) by increasing the pH to 9~10 with a 25~28% solution of ammonium hydroxide under vigorous stirring. For the W or Mo-containing nanocomposites, the desired amount of ammonium metatungstate (or ammonium molybdate) was dissolved in the mixture with vigorous stirring before precipitation. The loading of WO_3 or MO_3 was 16 wt.% based on the weights of the other metal oxides. The resulting precipitates were aged at room temperature for 24 h. After filtration and washing, the obtained nanocomposites were dried at 105 °C for 12 h, followed by calcination in air at 600 °C for 2 h. Nanosized TiO_2 and ZrO_2 were purchased from Aladdin Industrial Corporation (Shanghai, China). The commercial HZSM-5 catalyst (Si/Al=25) was obtained from the Catalyst Plant of Nankai University (Tianjin, China). Transmission electron micrographs of the nanocomposites were carried out on a transmission electron microscope (TEM-100CX, JEOL Inc., Tokyo, Japan) at a 200 kV accelerating voltage. Powder X-ray diffraction (XRD) patterns of the nanocomposites were analyzed by an X-ray diffractometer (X'Pert Pro MPD, PANalytical B.V., Almelo, Netherlands) using Cu Kα radiation (λ = 1.54060 Å) at 40 kV and 40 mA. The diffraction patterns were registered from 2θ = 5–80° at a scanning rate of 2° min^{-1}. The crystalline phases of metal-oxide nanocomposites were identified by comparison with JCPDS files. Total acid amounts of the nanocomposites were determined by temperature-programmed desorption of NH_3 (NH_3-TPD)

(DAS-7000, Huasi Instrument Co. Ltd., Changsha, China) connected with a thermal conductivity detector (TCD), and the types of the acid sites and the Brønsted to Lewis acid site ratio of the nanocomposites were determined by the adsorption of pyridine followed by the recording of their Fourier transform infrared (FTIR) spectra on a Frontier spectrometer (PerkinElmer Inc., Boston, USA), the concentrations of Brønsted and Lewis acid sites were subsequently calculated according to the method described by literature (Emeis, 1993; Tamura et al., 2012; Weingarten et al., 2011). The temperature-programmed measurements for the desorption of CO_2 (CO_2-TPD) of the nanocomposites were performed in a DAS-7000 (Huasi Instrument Co. Ltd., Changsha, China).

Catalytic fast pyrolysis and product analysis

Xylan and cellulose were purchased from Macklin Inc. (Shanghai, China) and Sigma–Aldrich (St Louis, USA), respectively. Organosolv lignin was extracted from bagasse by organosolv fractionation according to our previous studies(Zheng et al., 2017; Zheng et al., 2018). Catalytic fast pyrolysis of the biomass and its major components was conducted in a commercial micropyrolyzer (Pyroprobe 5200, CDS Analytical, Oxford, PA, USA). The samples were mixed with nanocomposites in an agate mortar to ensure thorough mixing. A mixture with the desired catalyst-to-feedstock weight ratio was accurately weighed on an analytical balance to an accuracy of 0.001 mg (XP6152, Mettler-Toledo GmbH, Giessen, Germany), and the pyrolysis temperature, residence time, and heating rate were fixed to 600 °C, 20 s, and 10,000 K/s, respectively. The pyrolysis products were analyzed in-line by an Agilent 7890 series gas chromatograph (GC) coupled with an Agilent 5975 series mass-selective detector (MSD). The GC column used was a J&W DB1701 column with dimensions of 60 m × 250 μm × 0.25 μm. The major pyrolysis products were quantified using the external standard method according to the guidelines provided by Agilent. The calibration curves were obtained by injecting the

mixed standard solutions with at least five concentrations of the target compounds into the GC oven under the same operating conditions. The carbon yields of the target products from the CFP of lignin, xylan or cellulose are defined as the moles of carbon in the target products divided by the moles of carbon in the feedstocks. The carbon yields of the furans from the raw biomass were calculated by the moles of carbon in the furans divided by the moles of carbon in the hemicellulose and cellulose fractions of the raw biomass. The carbon yields of the aromatics or phenols from the CFP of the raw biomass were calculated by the moles of carbon in the aromatics or phenols divided by the moles of carbon in the lignin fraction of the raw biomass. The carbon yields of char/coke were obtained by the elemental analysis of spent catalysts.

Supplemental References

Branca, C., Di Blasi, C., and Galgano, A. (2012). Catalyst Screening for the Production of Furfural from Corncob Pyrolysis. Energ Fuel *26*, 1520-1530.

Branca, C., Galgano, A., Blasi, C., Esposito, M., and Di Blasi, C. (2011). H2SO4-Catalyzed Pyrolysis of Corncobs. Energ Fuel *25*, 359-369.

Chen, X., Chen, Y., Chen, Z., Zhu, D., Yang, H., Liu, P., Li, T., and Chen, H. (2018). Catalytic fast pyrolysis of cellulose to produce furan compounds with SAPO type catalysts. J Anal Appl Pyrol *129*, 53-60.

Edmunds, C.W., Mukarakate, C., Xu, M., Regmi, Y.N., Hamilton, C., Schaidle, J.A., Labbé, N., and Chmely, S.C. (2019). Vapor-Phase Stabilization of Biomass Pyrolysis Vapors Using Mixed-Metal Oxide Catalysts. ACS Sustain Chem Eng *7*, 7386-7394.

Emeis, C. (1993). Determination of integrated molar extinction coefficients for infrared absorption bands of pyridine adsorbed on solid acid catalysts. J Catal *141*, 347-354.

Lee, H.W., Kim, Y.-M., Jae, J., Sung, B.H., Jung, S.-C., Kim, S.C., Jeon, J.-K., and Park, Y.-K. (2016). Catalytic pyrolysis of lignin using a two-stage fixed bed reactor comprised of in-situ natural zeolite and ex-situ HZSM-5. J Anal Appl Pyrol *122*, 282-288.

Lu, Q., Dong, C.-q., Zhang, X.-m., Tian, H.-y., Yang, Y.-p., and Zhu, X.-f. (2011). Selective fast pyrolysis of biomass impregnated with ZnCl2 to produce furfural: Analytical Py-GC/MS study. J Anal Appl Pyrol *90*, 204-212.

Lu, Q., Wang, Z.-x., Guo, H.-q., Li, K., Zhang, Z.-x., Cui, M.-s., and Yang, Y.-p. (2019). Selective preparation of monocyclic aromatic hydrocarbons from ex-situ catalytic fast pyrolysis of pine over Ti(SO4)2-Mo2N/HZSM-5 catalyst. Fuel *243*, 88-96.

Mihalcik, D.J., Mullen, C.A., and Boateng, A.A. (2011). Screening acidic zeolites for catalytic fast pyrolysis of biomass and its components. J Anal Appl Pyrol *92*, 224-232.

Mullen, C.A., and Boateng, A.A. (2010). Catalytic pyrolysis-GC/MS of lignin from several sources. Fuel Process Technol *91*, 1446-1458.

Murugappan, K., Mukarakate, C., Budhi, S., Shetty, M., Nimlos, M.R., and Román-Leshkov, Y. (2016). Supported molybdenum oxides as effective catalysts for the catalytic fast pyrolysis of lignocellulosic biomass. Green Chem *18*, 5548-5557.
Tamura, M., Shimizu, K.-i., and Satsuma, A. (2012). Comprehensive IR study on acid/base properties of metal oxides. Appl Catal A-Gen *433-434*, 135-145.
Wang, K., Kim, K.H., and Brown, R.C. (2014). Catalytic pyrolysis of individual components of lignocellulosic biomass. Green Chem *16*, 727-735.
Wang, K., Zhang, J., Shanks, B.H., and Brown, R.C. (2015). The deleterious effect of inorganic salts on hydrocarbon yields from catalytic pyrolysis of lignocellulosic biomass and its mitigation. Appl Energ *148*, 115-120.
Weingarten, R., Tompsett, G.A., Conner Jr, W.C., and Huber, G.W. (2011). Design of solid acid catalysts for aqueous-phase dehydration of carbohydrates: The role of Lewis and Brønsted acid sites. J Catal *279*, 174-182.
Zhang, H., Liu, X., Lu, M., Hu, X., Lu, L., Tian, X., and Ji, J. (2014). Role of Brønsted acid in selective production of furfural in biomass pyrolysis. Bioresource Technol *169*, 800-803.
Zheng, A., Chen, T., Sun, J., Jiang, L., Wu, J., Zhao, Z., Huang, Z., Zhao, K., Wei, G., He, F.*, et al.* (2017). Toward fast pyrolysis-based biorefinery: selective production of platform chemicals from biomass by organosolv fractionation coupled with fast pyrolysis. ACS Sustain Chem Eng *5*, 6507-6516.
Zheng, A.Q., Zhao, K., Sun, J.W., Jiang, L.Q., Zhao, Z.L., Huang, Z., Wei, G.Q., He, F., and Li, H.B. (2018). Effect of microwave-assisted organosolv fractionation on the chemical structure and decoupling pyrolysis behaviors of waste biomass. J Anal Appl Pyrol *131*, 120-127.